

Communication

Dual-Emission Carbon-Dot Ratiometric Fluorescence Sensor for Morphine Recognition in Biological Samples

Qinhong Yin ¹, Yijie Wang ², Xuerong Li ², Dezhi Yang ², Yaling Yang ², Cheng Yang ¹ and Yanqin Zhu ^{3,*}¹ Faculty of Narcotics Control, Yunnan Police College, Kunming 650223, China² Faculty of Life Science and Technology, Kunming University of Science and Technology, Kunming 650500, China³ Research Center for Analysis and Measurement, Kunming University of Science and Technology, Kunming 650093, China

* Correspondence: 20070029@kust.edu.cn

Abstract: Herein, a novel nitr[ogen-doped carbon dot (N-CD) fluorescence sensor with a dual emission ratio is developed using the microwave-assisted synthesis of m-phenylenediamine and spermidine. As a result of the fluorescence inner filtration effect (IFE) effect between morphine (MOR) and N-CD, the blue fluorescence of N-CDs at 350 nm was reduced in the presence of MOR, whereas the fluorescence of N-CDs at 456 nm increased substantially. The results demonstrated that the approach has a tremendous potential and that the linear range of MOR detection is 0.25–25 µg/mL, with a 71.8 ng/mL detection limit. Under UV light, the blue fluorescent system is easily visible to the naked eye. More significantly, the sensor proved successful in providing satisfactory results for the speciation measurement of MOR in a variety of biological samples.

Keywords: carbon dots; fluorescent sensor; dual-emission; morphine



Citation: Yin, Q.; Wang, Y.; Li, X.; Yang, D.; Yang, Y.; Yang, C.; Zhu, Y. Dual-Emission Carbon-Dot Ratiometric Fluorescence Sensor for Morphine Recognition in Biological Samples. *Biosensors* **2023**, *13*, 143.

<https://doi.org/10.3390/bios13010143>

Received: 13 December 2022

Revised: 11 January 2023

Accepted: 13 January 2023

Published: 15 January 2023



Copyright: © 2023 by the authors. Licensee MDPI, Basel, Switzerland. This article is an open access article distributed under the terms and conditions of the Creative Commons Attribution (CC BY) license (<https://creativecommons.org/licenses/by/4.0/>).

1. Introduction

An essential opium alkaloid known as morphine (MOR) is a natural source of a phenanthrene derivative purified from the *poppy* plant [1]. Clinically, it helps patients with pain relief, particularly chronic cancer symptoms. Regrettably, MOR can, like all opioids, lead to addiction and even death as a result of respiratory failure [2–5]. Overdose deaths caused by opioids claimed over 100,000 lives in the United States for the 12 months ending in April 2021, a 28.5% increase from the year before [6]. To monitor MOR levels in biological samples and prevent overdose or abuse-induced toxicity, morphine analysis is required in the healthcare and forensic domains [7].

It is generally accepted that MOR diagnosis uses two strategies: initial on-site screening and laboratory validation. The majority of the initial screening process involves qualitative analysis, which can immediately determine whether specimens contain morphine. The commonly used screening techniques include immunoassay, spectroscopy, and molecular imprinting [8–10]. These initial screening methods, although simple and fast, cannot be quantitatively analyzed and are also prone to false positive or false negative phenomena. For laboratory confirmation, samples are sent to the laboratory for further quantitative analysis using large instruments such as HPLC-MS (High-Performance Liquid Chromatography-Mass Spectrometry) [11,12] and GC-MS (Gas Chromatography-Mass Spectrometry) [13,14]. However, these instruments are bulky and require professional personnel to operate, so they cannot be used for rapid detection in the field of front-line law enforcement.

The fluorescence analysis method has been used more and more in field rapid detection due to its features of convenient operation, simple equipment, high sensitivity, and strong selectivity [15]. Carbon dots (CDs), generally termed semiconductor nanocrystals, are zero-dimensional nanocrystals, and the size is no more than twice the exciton Bohr

radius of the corresponding semiconductor material [16]. When the size reaches a critical value, the energy will be completely quantized, showing quantum characteristics, so it is called quantum dots. As a novel form of fluorescent semiconductor, quantum dots have many unique properties compared with traditional fluorescent dyes, such as good photostability, adjustable fluorescence emission wavelength, high fluorescence intensity, and good biocompatibility [17]. Because of their unique optical properties, they have gradually replaced the traditional organic fluorescent dyes and are a relatively ideal fluorescent nanomaterial. CDs have been used in detection and analysis more frequently due to their excellent fluorescence performance [18–20].

As the name implies, CDs are used in chemical sensors because of their molecular recognition function. However, fluorescent chemical sensors are usually interfered with or affected by sensor concentration, stability of detector or light source, and coexistence of components in a complex sample matrix [21]. The double emission ratio fluorescence method can avoid the above problems by using ratio fluorescence to detect the target [22]. It is still relatively uncommon to use carbon dots in the development of ratio fluorescence probes and to use CDs further in the detection of illegal drugs in biological samples.

In this study, novel carbon dots were synthesized from *m*-phenylenediamine and spermidine as the source of N atoms by microwave. Due to the improved inhibition efficiency attributed to the fluorophore's inner filter effect of the nanoparticles in the occurrence of MOR, the fluorescence detector was modified for the analysis of MOR. For the highly selective MOR measurement in biological samples, the dual emission ratio fluorescence sensor has been successfully employed.

2. Materials and Methods

2.1. Chemicals

All reagents and chemicals were analytical grade ($\geq 99.0\%$ purity) and were utilized as received without additional purification. The Ministry of Public Security's Key Laboratory of Narcotics Assay and Control Technology supplied MOR, heroin and methylamphetamine standards ($\geq 99.5\%$ purity). Spermidine (99.0% purity) and *m*-phenylenediamine (99.0% purity) were provided by Yuanye Biotechnology Co., Ltd., and Aladdin Biochemical Technology Co., Ltd., both of Shanghai, China. Siens Biochemical Technology Co., Ltd. and Maclean Biochemical Technology Co., Ltd. (Shanghai, China) provided the amino acids ($\geq 98.0\%$ purity) used in the interference test (Tianjin, China). All other chemicals were purchased from Zhiyuan Chemical Reagent Co., Ltd. and Fengchuan Chemical Reagent Technologies (Tianjin, China). Using the Milli-Q filtration apparatus (Millipore, Bedford, MA, USA), double-distilled water (18.2 M Ω cm) was utilized as the input to generate deionized water.

2.2. Instruments

A quartz cell (1 cm \times 1 cm)-equipped Agilent G9800A Cary Eclipse fluorescence spectrophotometer (USA) was applied to record the fluorescence spectrum. The emission and excitation monochromatic slit widths were both fixed at 10 nm. A TENSOR-27 FTIR spectrometer was used to record the FT-IR spectrum (Bruker, Bremen, Germany). Utilizing a UV-2550 spectrophotometer, the ultraviolet-visible (UV-vis) spectrum was recorded (Shimadzu, Kyoto, Japan). PHI5000 Versa Probeq-II with monochromatized Al K light was used to characterize X-ray photoelectron spectroscopy (XPS) (ULVAC-PHI, Kanagawa, Japan). X-ray diffraction (XRD) patterns were recorded by a PANalytical X'pert³ powder diffractometer using Ni-filtered Cu *K* α radiation. Using a transmission electron microscope, TecnaiG2 F30 S-Twin (FEI, Hillsboro, OR, USA) was applied to analyze the size and appearance of carbon dots. Carbon dots were synthesized using the Analytik-Jena TOPwave microwave-assisted digesting system (Jena, Germany). Using a Leici PHS-3 digital pH meter, the pH was controlled (Shanghai, China).

2.3. Preparation of Real Samples and Standard Solutions

In this study, blood samples were collected from healthy individuals. To collect serum at 4 °C for the plasma preparation, blood samples were centrifuged at 4000 rpm for 30 min. In water, a stock standard solution of MOR (100 µg/mL) was prepared. The stock standard solutions were diluted with deionized water to formulate working solutions. All solutions were kept in a freezer at 4 °C.

2.4. Preparation of N-CDs

The fluorescent N-CD schematic diagram for the synthesis process is shown in Figure 1. Spermidine (0.4 g) and m-phenylenediamine (0.4 g) were precisely weighed, dissolved in 40 mL of deionized water, and then heated at 180 °C for one hour in a microwave. Using a 0.22 µm filter membrane, the sample was filtered, and the filtrate was collected for dialyzing. The fractions corresponding to 3 kDa were ultrafiltered from N-CDs and studied in our work.

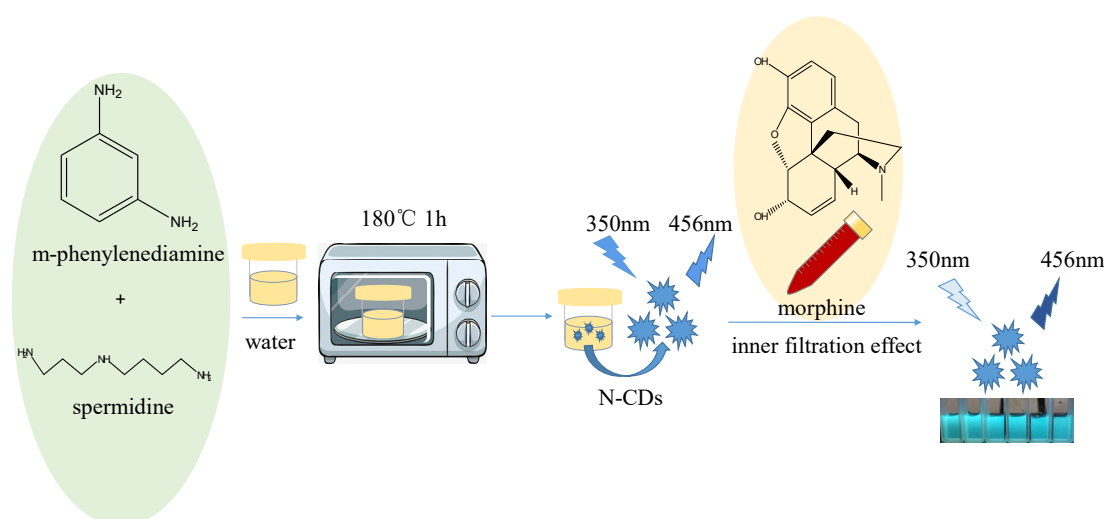


Figure 1. A schematic illustrating the synthesis and morphine detection of N-CDs.

2.5. Detection of MOR with the Ratiometric Sensor

At room temperature, 100 µL of N-CDs solution and 20 µL of serum with various concentrations of MOR were carefully mixed. Under the optimized conditions, the pH was adjusted to 8 with citrate-disodium hydrogen phosphate buffer. Next, the mixture was diluted to 4 mL with deionized water and heated in a water bath at 44 °C to maximize the sensitivity. The final MOR concentrations were 0.25, 0.5, 1.0, 1.25, 2.5, 5, 10 and 25 µg/mL. Then, with excitation at 310 nm, fluorescence spectra in the wavelength range of 330–470 nm were obtained. This sensing system's MOR selectivity was evaluated using NO_2^- , HCO_3^- , K^+ , Na^+ , Mg^{2+} , Cu^{2+} , K^+ , Fe^{2+} , Mn^{2+} , Zn^{2+} and other amino acids, such as Tyr, Gly, Try, Leu, Met, Glu, Lys, and Cys.

3. Results and Discussion

3.1. Characterization Results of N-CDs

TEM was used to analyze the nanostructure of N-CDs. N-CD TEM images at various scales are displayed in Figure 2A,B. As shown in Figure 2A, the transmission TEM images show good monodispersity and good size homogeneity of N-CDs, clearly indicating that these nanoparticles are almost spherical with an average size of 5 nm. However, neither Figure 2A nor Figure 2B showed any obvious lattice fringes, suggesting that the crystallinity of the carbon dots is weak, which is in accordance with previous research [23,24].

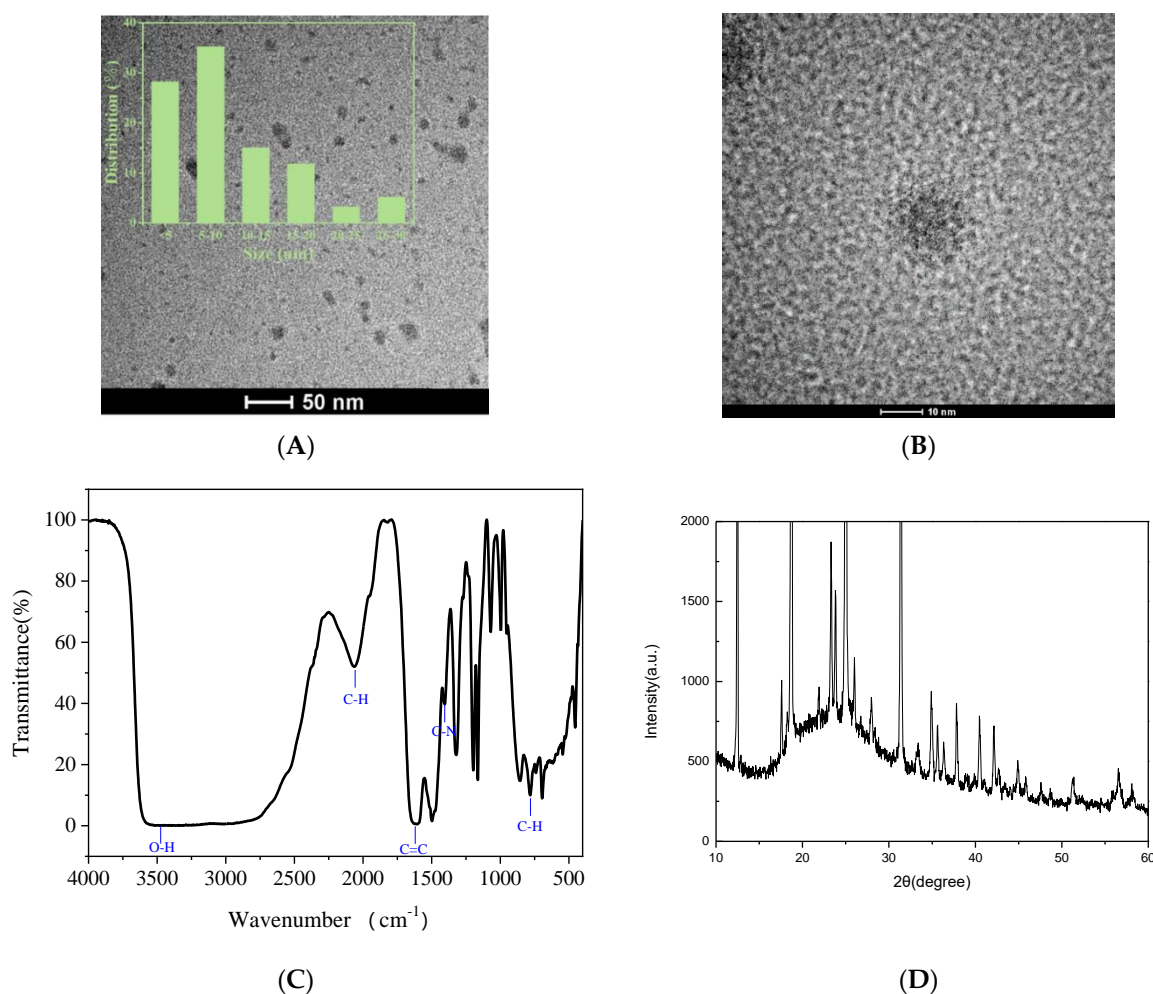


Figure 2. The analysis of N-CDs using (A) particle size distribution and (B) TEM images at different scales; (C) FT-IR; (D) XRD.

The N-CD FT-IR spectra are shown in Figure 2C. The stretching vibrations of O-H and N-H are associated with the low-intensity band at 3472 cm^{-1} . The C-H stretching and bending vibrations were demonstrated by the peaks at 2065 cm^{-1} and 732 cm^{-1} , respectively [25]. The C=C and C-N bending vibrations are correlated to the peaks at 1605 and 1424 cm^{-1} , respectively [26]. These results confirmed the existence of the -NH₂, C-N, and C=C groups, which enhanced the solubility of N-CDs in water.

Figure 2D shows the XRD patterns of the obtained material. As can be seen, it has an amorphous structure with a broad peak at $2\theta = 21.22^\circ$ that is clearly related to the amorphous nature of C-dots.

XPS was applied to investigate the chemical groups on the surface of N-CDs. C1s, N1s, and O1s concentration levels are the origin of the peaks in the spectrum at 283.2, 399.2, and 530.4 eV (Figure 3A). Three peaks in the C1s spectra can be assigned to the C=C, C-N, and C=O groups with energies of 284.8, 286.2, and 288.8 eV, respectively (Figure 3B) [27]. Two peaks in the N1s spectra were observed at 399.2 and 401.3 eV (Figure 3C), and they might belong to N-H and N-O bond types. Two major peaks from the C=O and C-O groups can be observed at 532.0 and 533.7 eV, according to further analysis of the O1s spectra (Figure 3D) [28]. Additionally, quantum yield (QY) of N-CDs was determined based on the relative method by using quinine sulfate as reference (dissolved in 0.1 M H₂SO₄, QY = 54.6%) [29]. According to the reference calculation formula, the N-CD quantum yield was 12.95%.

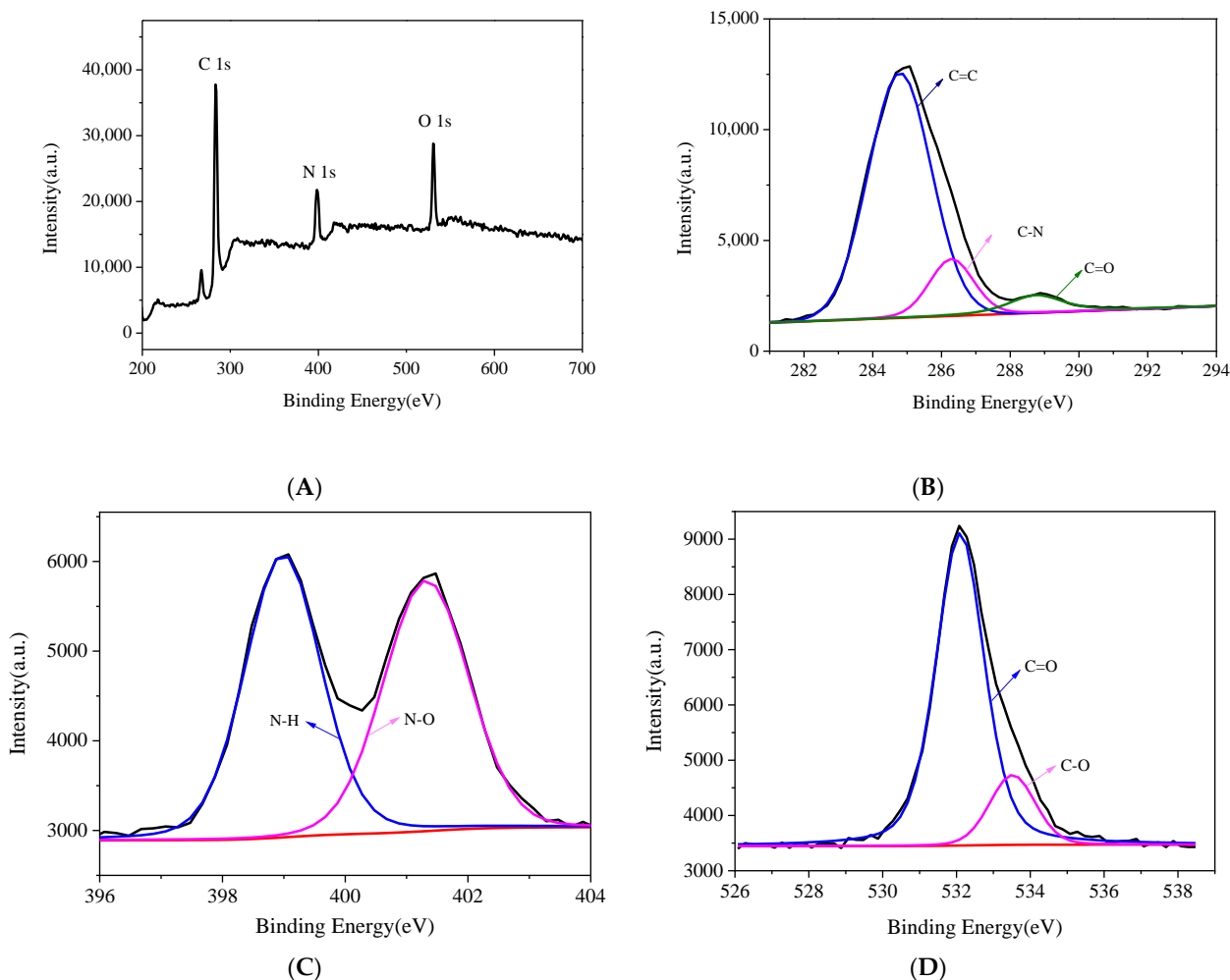


Figure 3. (A) XPS spectra of N-CDs, high resolution (B) C 1s, (C) N 1s, and (D) O 1s peaks of N-CDs.

3.2. Optical Properties of N-CDs

Figure 4A shows the N-CDs' UV-vis spectrum. The π - π^* transitions are responsible for the shoulder peak at 242 nm [30]. Besides the peak at 242 nm, no sharp absorption peaks were present for N-CDs, except for the display of a long absorption edge, which was extended from 275 to 400 nm. Using the same 310 nm excitation wavelength, N-CDs in this sensor system displayed two emission peaks (350 nm and 456 nm) (Figure 4B).

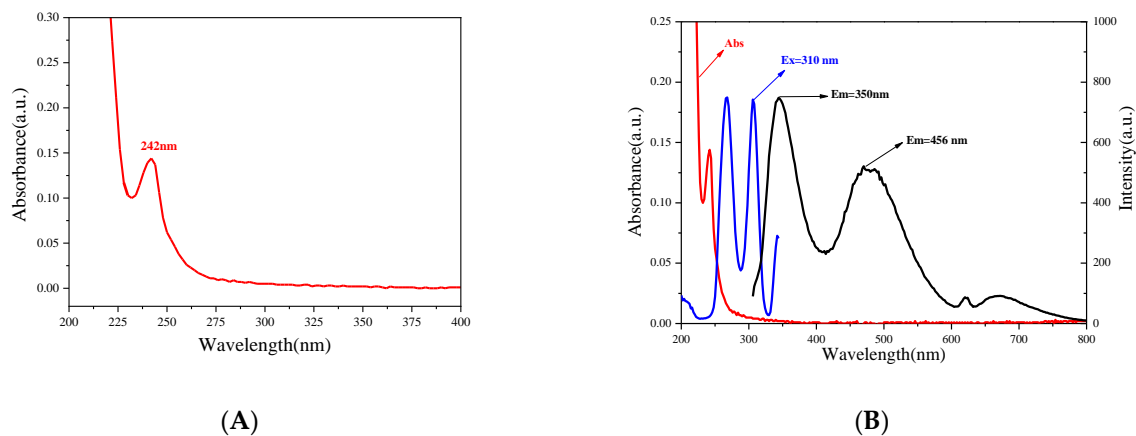


Figure 4. (A) UV-Vis absorption spectra of N-CDs; (B) fluorescence spectra of N-CDs.

3.3. Effect of Solution pH

Fluorophore ionization has a significant impact on how much light is emitted. Since the I_{350}/I_{456} value decreases with increasing concentration of MOR, it is necessary to adjust the solution pH to maximize a method's sensitivity. To maximize a method's sensitivity, it is necessary to adjust the pH of a solution. The pH ranged in this study from 6.0 to 9.0. I_{350}/I_{456} 's fluorescence ratio increased from pH 8.0 to 9.0 after declining from pH 6.0 to 8.0. (Figure 5A). Therefore, before testing, the pH value of the test solution must be adjusted to 8.0.

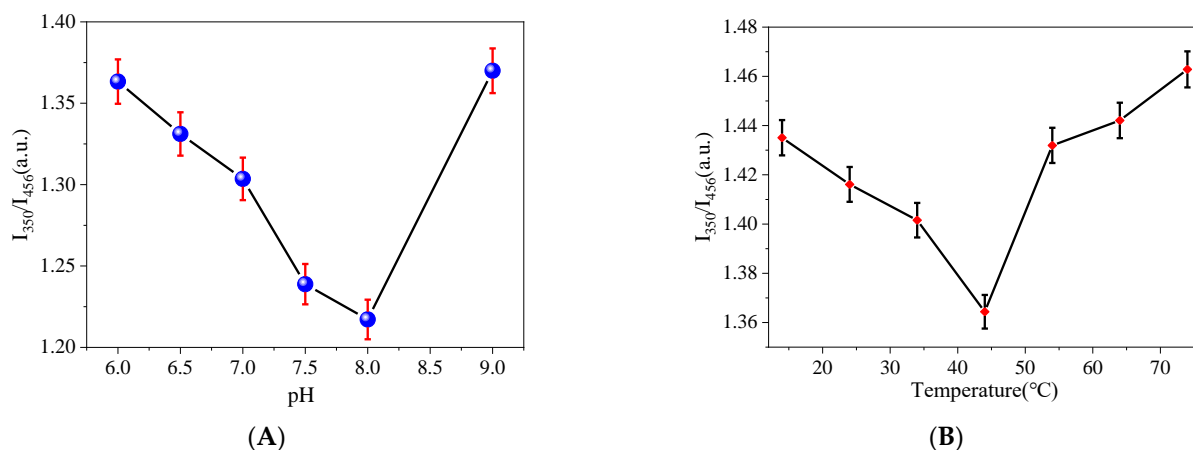


Figure 5. Effect of (A) pH under the same conditions (system temperature: 44 °C; N-CDs: 100 μ L; MOR concentration: 10 μ g/mL; Ex: 310 nm; Em: 350 nm and 456 nm) and (B) system temperature under the same conditions (pH: 8.0; N-CDs: 100 μ L; MOR concentration: 10 μ g/mL; Ex: 310 nm; Em: 350 nm and 456 nm).

3.4. System Temperature

Temperature has an effect on the return of excited electrons to the ground state to produce changes in fluorescence intensity. Thus, the effects of system temperatures of 14, 24, 34, 44, 54, 64, and 74 °C on the fluorescence intensity were explored (Figure 5B). The results show that the fluorescence ratio of I_{350}/I_{456} decreased from 14 °C to 44 °C and then increased when the temperature increased from 44 °C to 74 °C. Considering this comprehensively, the temperature of the system was chosen at room 44 °C. The temperature change feature could be attributed to the temperature-enhanced population of non-radiative channels of surface (trap/defect) states. More non-radiative channels would be activated at a higher temperature, and more excited electrons returned to the ground state via a non-radiative process, resulting in decreased fluorescence intensity [31,32].

3.5. Effect of Interfering Ions and Substances

An innovative fluorescence probe must have excellent selectivity. The effects of different ions (NO_2^- , HCO_3^- , Na^+ , Mg^{2+} , Cu^{2+} , K^+ , Fe^{2+} , Mn^{2+} , Zn^{2+} , Fe^{3+}) and interfering substances (tyrosine, glycine, tryptophan, leucine, methionine, glutathione, glucose, lysine, cysteine and vitamin C) added in the same proportion (100 μ g/mL) on the fluorescence signal of the morphine+N-CDs system were explored. Experiments were carried out three times in regard to the results displayed in Figure 6A,B. These interfering ions and interfering substances did not affect the system. The systematic execution of N-CDs concerning their selectivity towards MOR was also conducted against some of the very common interfering MOR analogues such as heroin and methylamphetamine. It was found that morphine significantly enhanced the fluorescence of N-CDs at 466 nm, while heroin and methamphetamine had no effect on N-CDs at 466 nm (Figure 6C). The above results confirm the good selectivity of the ratiometric fluorescence sensor toward MOR.

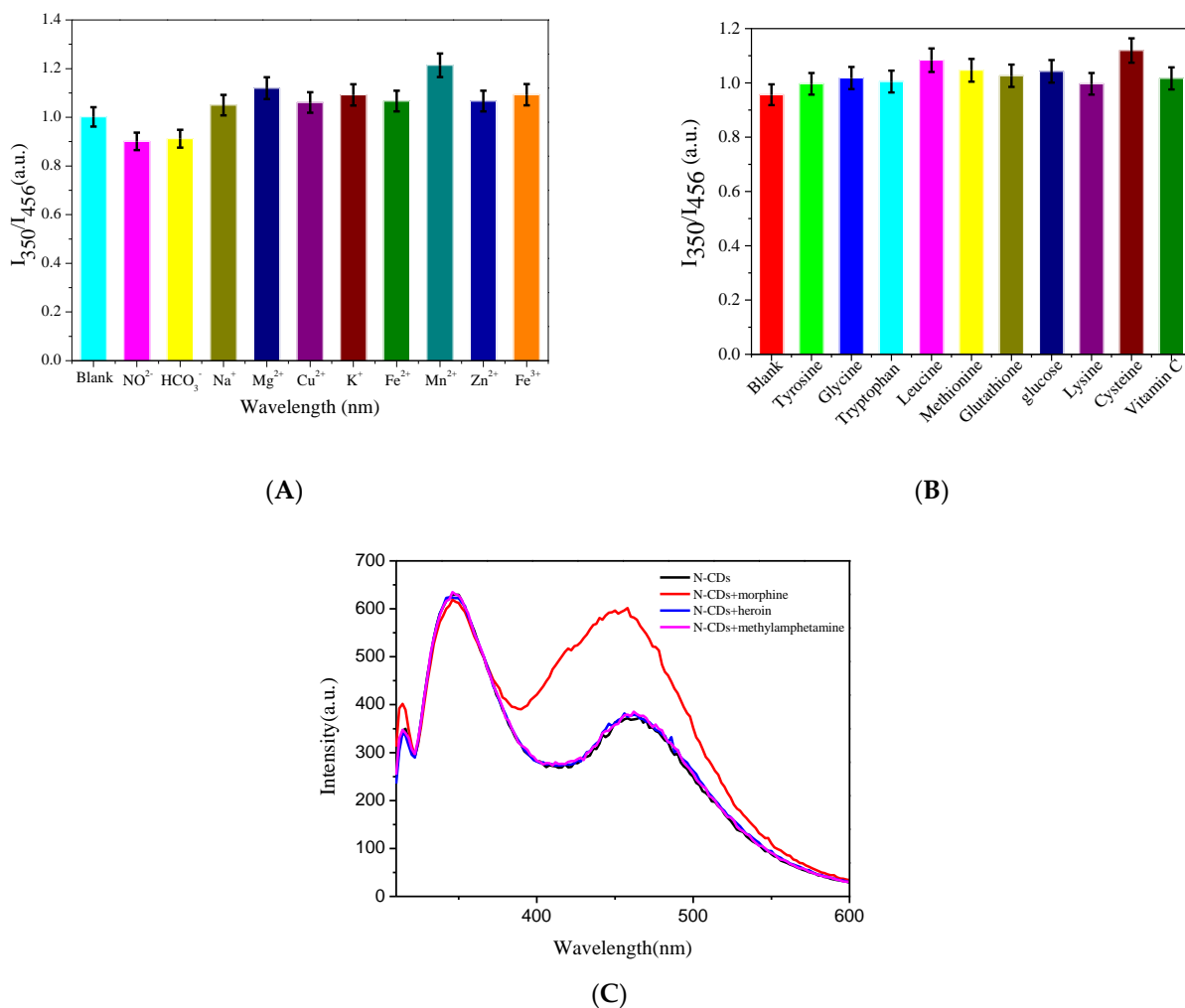


Figure 6. Effect of (A) interfering ions and (B) interfering substances under the same conditions (pH: 8.0; system temperature: 44 °C; N-CDs: 100 μL ; MOR concentration: 10 $\mu\text{g}/\text{mL}$; Ex: 310 nm; Em: 350 nm and 456 nm) ($n = 3$); (C) fluorescence spectra of MOR and its analogues (pH: 8.0; system temperature: 44 °C; N-CDs: 100 μL ; concentration of MOR and its analogues: 10 $\mu\text{g}/\text{mL}$).

3.6. Method Validation

The concentration of MOR displayed a consistent pattern as a function of I_{350}/I_{456} in the range of 0.25–25 $\mu\text{g}/\text{mL}$ ($I_{350}/I_{456} = 1.6027 - 0.02622C$, $R^2 = 0.9910$) under optimal conditions (Figure 7). Error bars in the calibration curve were obtained from three parallel measurements. The method's LOD was determined to be 71.8 ng/mL using the formula $3s/K$ (s is the continuous determination standard deviation of 10 blanks, and K is the slope of the calibration trendline), and the relative standard deviation (RSD) was 4.6% ($c = 5 \mu\text{g}/\text{mL}$, $n = 8$), in accordance with the IUPAC standard [33]. Based on this, the limit of quantitation (LOQ) of MOR determined by this sensor was calculated to be 0.239 $\mu\text{g}/\text{mL}$ by $10s/k$. This approach exhibited a comparable detection limit to earlier reported MOR probes based on CDs, but it had a higher selectivity [34–38].

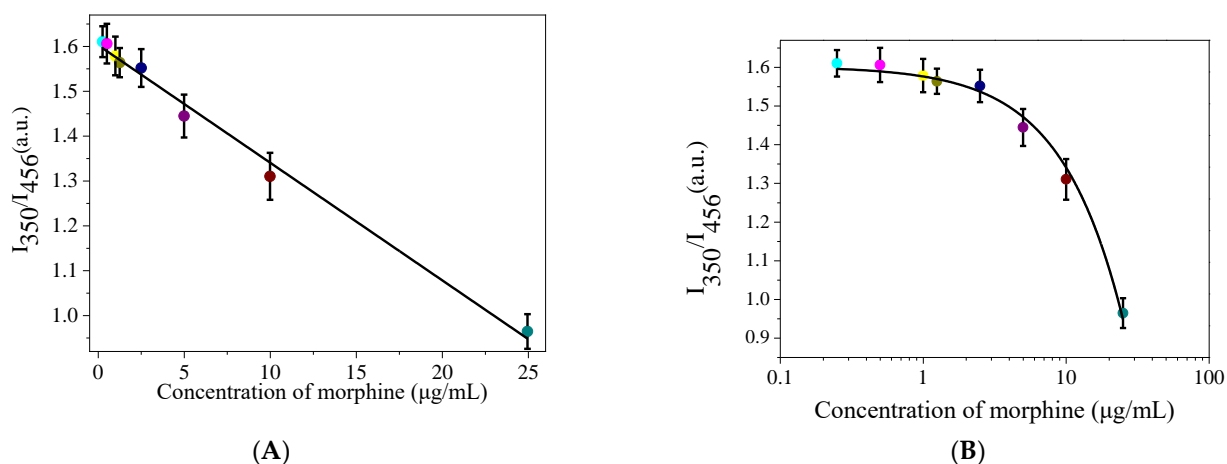


Figure 7. (A) A linear plot of I_{350}/I_{456} versus the concentration of morphine in the range of 0.25–25 $\mu\text{g/mL}$ ($n = 3$); (B) Fitted curves of I_{350}/I_{456} versus the morphine concentration plotted on a log scale.

3.7. Analysis of Real Samples

Considering the complexity of blood samples, we added morphine to blood samples in this study to verify the accuracy and anti-interference of the method. Actual blood samples from patients were tested using the standardized calibration curve. The suggested method was used to determine the amounts of MOR in various blood samples (Table 1). The innovative fluorescent approach used had a recovery of between 93.8% and 103.3% with RSDs of under 6%. The analytical data of several strategies for MOR detection are evaluated in Table 2. The outcomes reveal that the proposed approach can be used to swiftly test blood for illegal drugs using the methods outlined. The results confirmed that the proposed method showed good anti-interference and accuracy.

Table 1. Quantification of MOR in samples ($n = 3$).

Samples	Added ($\mu\text{g/mL}$)	Found ($\mu\text{g/mL}$)	Recovery (%)	RSD (%)
Blood (female)	-	N. D. ^a	-	-
	2.495	2.411	96.7	5.6
	4.990	5.153	103.3	4.3
Blood (male)	-	N. D. ^a	-	-
	2.495	2.515	100.8	3.5
	4.990	4.683	93.8	4.9

^a Not detected.

Table 2. The overview of analytical data of the reported methods for the analysis of MOR.

Materials	Detection Method	Linearity Range	LOD	Reference
graphene quantum dots	voltammetric electrode	0–3.5 μM	0.06 μM	[34]
chiral colloidal CdSe quantum dots	fluorescence enhancement	/	0.06 μM	[35]
graphene quantum dots	fluorescence enhancement	0–33 μM	0.5 $\mu\text{g/mL}$	[36]
anti-morphine antibody-labeled C-Dots	fluorescence immunoassay	3.2×10^{-4} –10 mg/L	3.0×10^{-4} mg/L	[37]
N,Cl-CDs	fluorescence enhancement	0.15–280.25 $\mu\text{g/mL}$	46.5 ng/mL	[38]
N-CDs	fluorescence quenching	0.25–25 $\mu\text{g/mL}$	71.8 ng/mL	This work

3.8. Sensing Mechanism of Ratiometric Nanosensor towards MOR

We performed a series of tests to examine the effects of various MOR substances in the N-CDs system, and the results are shown in Figure 8A. These tests were carried out to investigate the potential mechanism of the N-CDs/MOR based fluorescence sensing

technique for MOR analysis. The fluorescence of N-CDs at 350 nm was reduced when the MOR was introduced, whereas the fluorescence of N-CDs at 456 nm was substantially enhanced. The absorbance peak of MOR aligns with the emission spectrum of N-CDs, as shown in Figure 8A, demonstrating the possible existence of an inner filtration effect (IFE) or Förster resonance energy transfer (FRET) between N-CDs and MOR [39,40]. As a result, the intensity of the N-CDs fluorescence emission gradually decreased with the addition of morphine. As a result of the comparatively small size distribution of the resulting N-CDs, Figure 4B also exhibits a narrow band at 300–400 nm in the emission spectra. To further confirm the sensing mechanism, a fluorescence lifetime experiment was conducted [41]. Figure 8B shows the fluorescence lifetime graph. The average lifetime of fluorescence is 2.25 ns ($\chi^2 = 0.90$), while the lifetime components of N-CDs are $\tau_1 = 0.83$ ns (26.15%) and $\tau_2 = 2.42$ ns (73.85%). The mean fluorescence lifetime is 2.83 ns ($\chi^2 = 0.94$), and the lifetime components after the addition of morphine are $\tau_1 = 0.86$ ns (23.76%) and $\tau_2 = 3.01$ ns (76.24%). These results show that the fluorescence lifetime is essentially unaffected by the presence or absence of MOR. This indicates that IFE, not FRET, causes fluorescence quenching because the donor's PL lifetime is constant during IFE but seems to change significantly during FRET. As a result, we can conclude that MOR and N-CDs have an IFE effect [42].

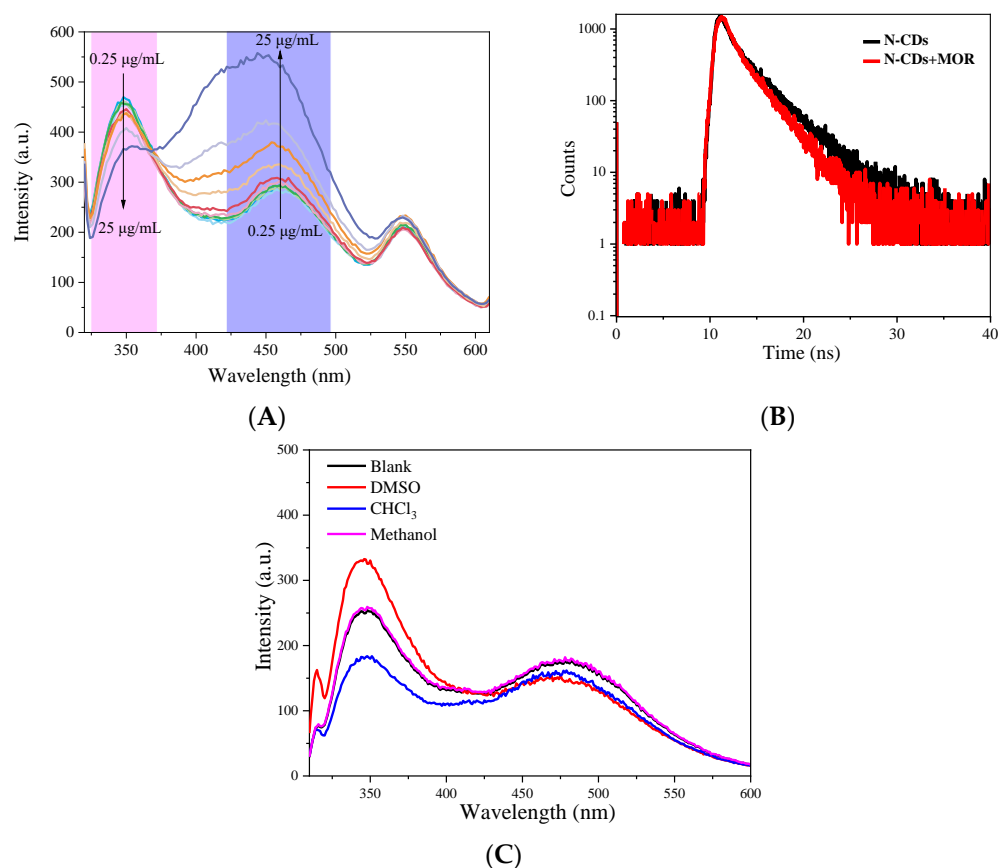


Figure 8. (A) Fluorescence spectra of N-CD solution with different concentrations of morphine. (B) The fluorescence lifetime curve of N-CDs and N-CDs + morphine. (C) The fluorescence spectra of N-CDs in different apolar solvents.

Since FRET is not affected by the polarity of the solvent, changing the polarity of the solution has little effect on the quenching efficiency based on FRET. Therefore, we also studied the interaction of N-CDs in different apolar solvents (Figure 8C). The experimental results show that the fluorescence is dramatically changed in dimethylsulfoxide (DMSO) and chloroform (CHCl₃). This further confirms that the interaction mechanism between N-CDs and MOR might be due to IFE.

4. Conclusions

In this study, a simple and accurate ratiometric fluorescence sensor for MOR measurement between N-CDs and MOR was developed. Based on the FRET effect, the addition of MOR further inhibited the fluorescence of N-CDs. High sensitivity, superior selectivity, rapid detection, and an expanded linear response range were all promising characteristics of the dual-emission carbon-dot ratiometric fluorescence sensing device. The detection of MOR in actual blood samples was evidence of the developed method.

Author Contributions: Q.Y.: Characterization, data analysis and writing. Y.W.: Probe synthesis, selectivity sensitivity and data analysis. X.L.: Conceptualization, supervision and data analysis. D.Y.: morphine detection in real samples, preparation of N-CDs composite hydrogels and CQD-based test papers. Y.Y. and C.Y.: Manuscript editing and data analysis. Y.Z.: original draft and editing, manuscript review. All authors have read and agreed to the published version of the manuscript.

Funding: This work was supported by National Natural Science Foundation of China (No. 82260337), National Innovation and Entrepreneurship Training Program for College Student of China (No. 202111392006), the Opening Project of Key Laboratory of Ministry of Public Security for Drug Analysis and Anti-Drug Technology (No. YNPC-B2021004) and Basic Research Project of Yunnan Province/General Project (No. 202001AT070002).

Institutional Review Board Statement: Not applicable.

Informed Consent Statement: Not applicable.

Data Availability Statement: Not applicable.

Conflicts of Interest: The authors declare no conflict of interest.

References

1. Acharya, H.S.; Sharma, V. Molecular characterization of opium poppy (*Papaver somniferum*) germplasm. *Am. J. Infect. Dis.* **2009**, *5*, 148–153. [[CrossRef](#)]
2. Pandey, S.S.; Singh, S.; Babu, C.S.V.; Shanker, K.; Srivastava, N.K.; Shukla, A.K.; Kalra, A. Fungal endophytes of catharanthus roseus enhance vindoline content by modulating structural and regulatory genes related to terpenoid indole alkaloid biosynthesis. *Sci. Rep.* **2016**, *6*, 26583. [[CrossRef](#)]
3. Celik, I.; Camci, H.; Kose, A.; Kosar, F.C.; Doganlar, S.; Frary, A. Molecular genetic diversity and association mapping of morphine content and agronomic traits in turkish opium poppy (*papaver somniferum*) germplasm. *Mol. Breed.* **2016**, *36*, 46. [[CrossRef](#)]
4. Brezinová, B.; Macák, M.; Eftimová, J. The morphological diversity of selected traits of world collection of poppy genotypes (genus *Papaver*). *J. Cent. Eur. Agric.* **2009**, *10*, 183–192.
5. Bandoni, A.L.; Stermitz, F.R.; Rondina, R.; Coussio, J.D. Alkaloidal content of argentine argemone. *Phytochemistry* **1975**, *14*, 1785–1788. [[CrossRef](#)]
6. Pham, Q.; Burrows, M.; Litwin, A. Urgent need to expand syringe services programs in South Carolina and beyond. *Subst. Abuse Treat. Pre. Policy* **2022**, *17*, 47. [[CrossRef](#)] [[PubMed](#)]
7. Alhaddad, M.; Sheta, S.M. Dual naked-eye and optical chemosensor for morphine detection in biological real samples based on Cr (iii) metal-organic framework nanoparticles. *ACS Omega* **2022**, *5*, 28296–28304. [[CrossRef](#)] [[PubMed](#)]
8. Lü, S.; Chang, W.B.; Li, Y.Z.; Ci, Y.X. The immunoassay of morphine using phase separation and colloid gold marking. *Chin. J. Anal. Chem.* **2000**, *28*, 1324–1325.
9. Feng, S.; Chen, W.; Huang, W.; Cheng, M.; Lin, J.; Li, Y. Surface-enhanced Raman spectroscopy of morphine in silver colloid. *Chin. Opt. Lett.* **2009**, *7*, 1055–1057. [[CrossRef](#)]
10. Vergara, A.V.; Pernites, R.B.; Tiu, B.D.B.T.; Leon, A.C.C.; Mangadlao, J.D.; Binag, C.A.; Advincula, R.C. Capacitive detection of morphine via cathodically electropolymerized, molecularly imprinted poly(p-aminostyrene) films. *Macromol. Chem. Phys.* **2016**, *217*, 1810–1822. [[CrossRef](#)]
11. Heydari, P.; Martins, M.; Rosing, H.; Hillebrand, M.; Gebretensae, A.; Schinkel, A.H.; Beijnen, J.H. Development and validation of a UPLC-MS/MS method with a broad linear dynamic range for the quantification of morphine, morphine-3-glucuronide and morphine-6-glucuronide in mouse plasma and tissue homogenates. *J. Chromatogr. B* **2021**, *1166*, 122403. [[CrossRef](#)] [[PubMed](#)]
12. Jin, Y.; Zhao, J.; Xu, X.; Wang, Y. Qualitative and quantitative analysis of opiate and related metabolites in human urine samples by UPLC-MS/MS. *Int. J. Mass Spectrom.* **2021**, *464*, 116575. [[CrossRef](#)]
13. Robert, M. GC-MS quantitation of codeine, morphine, 6-acetylmorphine, hydrocodone, hydromorphone, oxycodone, and oxymorphone in blood. *J. Anal. Toxicol.* **2005**, *29*, 301–308.
14. Santos, V.; López, K.J.; Santos, L.M.; Yonamine, M.; Carmona, M.J.; Santos, S.R. Determining plasma morphine levels using GC-MS after solid phase extraction to monitor drug levels in the postoperative period. *Clinics* **2008**, *63*, 307–314. [[CrossRef](#)]

15. Tian, Y.; Martinez, M.M.; Pappas, D. Fluorescence correlation spectroscopy: A review of biochemical and microfluidic applications. *Appl. Spectrosc.* **2011**, *65*, 115–124. [[CrossRef](#)]
16. Lim, S.Y.; Shen, W.; Gao, Z.Q. Carbon quantum dots and their applications. *Chem. Soc. Rev.* **2015**, *44*, 362–381. [[CrossRef](#)]
17. Sun, S.; Zhang, L.; Jiang, K.; Wu, A.; Lin, H. Toward high-efficient red emissive carbon dots: Facile preparation, unique properties, and applications as multifunctional theranostic agents. *Chem. Mater.* **2016**, *28*, 8659–8668. [[CrossRef](#)]
18. Wang, Y.; Zhu, Y.; Yu, S.; Jiang, C. Fluorescent carbon dots: Rational synthesis, tunable optical properties and analytical applications. *RSC Adv.* **2017**, *7*, 40973–40989. [[CrossRef](#)]
19. Zhang, D.; Zhang, F.; Liao, Y.; Wang, F.; Liu, H. Carbon quantum dots from pomelo peel as fluorescence probes for “turn-off-on” high-sensitivity detection of Fe³⁺ and L-cysteine. *Molecules* **2022**, *27*, 4099. [[CrossRef](#)]
20. Zhang, Q.; Du, S.; Tian, F.; Long, X.; Xie, S.; Tang, S.; Bao, L. Silver nanoparticle-functionalised nitrogen-doped carbon quantum dots for the highly efficient determination of uric acid. *Molecules* **2022**, *27*, 4586. [[CrossRef](#)]
21. Bhattacharyya, D.; Sarswat, P.K.; Free, M.L. Quantum dots and carbon dots based fluorescent sensors for TB biomarkers detection. *Vacuum* **2017**, *146*, 606–613. [[CrossRef](#)]
22. Wang, K.X.; Nie, C.; Guan, R.F.; Zhang, H. Double emission fluorescence probes based on unconventional fluorescent molecules and fluorescein isothiocyanate for ClO and Cu²⁺ detection. *Chin. J. Anal. Chem.* **2022**, *50*, 47–54. [[CrossRef](#)]
23. Xu, D.; Fang, L.; Chen, H.; Yin, L.; Ying, S.; Xie, J. One-step hydrothermal synthesis and optical properties of self-quenching-resistant carbon dots towards fluorescent ink and as nanosensors for Fe³⁺ detection. *RSC Adv.* **2019**, *9*, 8290–8299. [[CrossRef](#)] [[PubMed](#)]
24. Li, S.; Yang, H.; Xu, R.; Jiang, Y.; Gong, Y.; Gu, L.; Yu, Y. Selenium embedded in MOFs-derived N-doped microporous carbon polyhedrons as a high performance cathode for sodium-selenium batteries. *Mater. Chem. Front.* **2018**, *2*, 1574–1582. [[CrossRef](#)]
25. Wang, Y.; Chang, Q.; Hu, S. Carbon dots with concentration-tunable multicolored photoluminescence for simultaneous detection of Fe³⁺ and Cu²⁺ ions. *Sensor. Actuat. B* **2017**, *253*, 928–933. [[CrossRef](#)]
26. Cheng, Y.; Li, C.M.; Mu, R.Z.; Li, Y.F.; Xing, T.T.; Chen, B.B.; Huang, C.Z. Dynamically long-term imaging of cellular RNA by fluorescent carbon dots with surface isoquinoline moieties and amines. *Anal. Chem.* **2018**, *90*, 11358–11365. [[CrossRef](#)] [[PubMed](#)]
27. Gao, Z.; Li, X.; Shi, L.; Yang, Y. Deep eutectic solvents-derived carbon dots for detection of mercury (ii), photocatalytic antifungal activity and fluorescent labeling for *C. albicans*. *Spectrochim. Acta A* **2019**, *220*, 117080. [[CrossRef](#)] [[PubMed](#)]
28. Wang, H.; Liu, S.; Xie, Y.; Bi, J.; Li, Y.; Song, Y.; Cheng, S.; Li, D.; Tan, M. Facile one-step synthesis of highly luminescent n-doped carbon dots as an efficient fluorescent probe for chromium(vi) detection based on the inner filter effect. *New J. Chem.* **2018**, *42*, 3729–3735. [[CrossRef](#)]
29. Miao, C.F.; Guo, X.Z.; Zhang, X.T.; Lin, Y.N.; Han, W.D.; Huang, Z.J.; Wen, S.H. Ratiometric fluorescence assay based on carbon dots and Cu²⁺-catalyzed oxidation of *O*-phenylenediamine for the effective detection of deferasirox. *RSC Adv.* **2021**, *11*, 34525–34532. [[CrossRef](#)]
30. Liu, J.; Liu, X.; Luo, H.; Gao, Y. One-step preparation of nitrogen-doped and surface-passivated carbon quantum dots with high quantum yield and excellent optical properties. *RSC Adv.* **2014**, *4*, 7648–7654. [[CrossRef](#)]
31. Eda, G.; Lin, Y.Y.; Mattevi, C.H.; Yamaguchi, H.; Chen, H.A.; Chen, I.S.; Chen, C.W.; Chhowalla, M. Blue photoluminescence from chemically derived graphene oxide. *Adv. Mater.* **2010**, *22*, 505–509. [[CrossRef](#)] [[PubMed](#)]
32. Hu, Y.; Yang, J.; Jia, L.; Yu, J.S. Ethanol in aqueous hydrogen peroxide solution: Hydrothermal synthesis of highly photoluminescent carbon dots as multi-functional nanosensors. *Carbon* **2015**, *93*, 999–1007. [[CrossRef](#)]
33. Peng, L.; Wei, R.; Li, K.; Zhou, Z.; Song, P.; Tong, A. A ratiometric fluorescent probe for hydrophobic proteins in aqueous solution based on aggregation-induced emission. *Analyst* **2013**, *138*, 2068–2072. [[CrossRef](#)] [[PubMed](#)]
34. Mokhtari, A.; Karimi-Maleh, H.; Ensafi, A.A.; Beitollahi, H. Application of modified multiwall carbon nanotubes paste electrode for simultaneous voltammetric determination of morphine and diclofenac in biological and pharmaceutical samples. *Sensor. Actuat. B* **2012**, *169*, 96–105. [[CrossRef](#)]
35. Masteri-Farahani, M.; Mosleh, N. Functionalization of graphene quantum dots with antimorphine: Design of selective nanosensor for detection of morphine. *Mater. Lett.* **2019**, *241*, 206–209. [[CrossRef](#)]
36. Masteri-Farahani, M.; Askari, F. Design and photophysical insights on graphene quantum dots for use as nanosensor in differentiating methamphetamine and morphine in solution. *Spectrochim. Acta A* **2019**, *206*, 448–453. [[CrossRef](#)]
37. Zhang, C.; Yu, X.; Shi, X.M.; Han, Y.F.; Guo, Z.M.; Liu, Y. Development of carbon quantum dot-labeled antibody fluorescence immunoassays for the detection of morphine in hot pot soup base. *Food Anal. Methods* **2020**, *13*, 1042–1049. [[CrossRef](#)]
38. Yin, Q.; Wang, M.; Fang, D.; Zhu, Y.; Yang, L. Novel N,Cl-doped deep eutectic solvents-based carbon dots as a selective fluorescent probe for determination of morphine in food. *RSC Adv.* **2021**, *11*, 16805–16813. [[CrossRef](#)]
39. Dai, R.; Hu, Y. Green/red dual emissive carbon dots for ratiometric fluorescence detection of acid red 18 in food. *Sensor. Actuat. B* **2022**, *370*, 132420. [[CrossRef](#)]
40. Wang, M.; Wang, M.; Zhang, F.; Su, X. A ratiometric fluorescent biosensor for the sensitive determination of α -glucosidase activity and acarbose based on N-doped carbon dots. *Analyst* **2020**, *145*, 5808–5815. [[CrossRef](#)]

41. Zhang, Z.; Huang, J.; Zhang, M.; Yuan, Q.; Dong, B. Ultrathin hexagonal SnS₂ nanosheets coupled with g-C₃N₄ nanosheets as 2D/2D heterojunction photocatalysts toward high photocatalytic activity. *Appl. Catal. B* **2015**, *163*, 298–305. [[CrossRef](#)]
42. You, J.; Liu, H.; Zhang, R.; Pan, Q.; Sun, A.; Zhang, Z.; Shi, X. Development and application of tricolor ratiometric fluorescence sensor based on molecular imprinted nanoparticles for visual detection of dibutyl phthalate in seawater and fish samples. *Sci. Total Environ.* **2022**, *848*, 157675. [[CrossRef](#)] [[PubMed](#)]

Disclaimer/Publisher's Note: The statements, opinions and data contained in all publications are solely those of the individual author(s) and contributor(s) and not of MDPI and/or the editor(s). MDPI and/or the editor(s) disclaim responsibility for any injury to people or property resulting from any ideas, methods, instructions or products referred to in the content.